A New Class of Highly Potent Matrix Metalloproteinase Inhibitors Based on Triazole-Substituted Hydroxamates: (Radio)Synthesis and in Vitro and First in Vivo Evaluation

Verena Hugenberg,*,[†] Hans-Jörg Breyholz,[†] Burkhard Riemann,[†] Sven Hermann,[‡] Otmar Schober,[†] Michael Schäfers,[‡,§] Umesh Gangadharmath,[∥] Vani Mocharla,[∥] Hartmuth Kolb,[∥] Joseph Walsh,[∥] Wei Zhang,[∥] Klaus Kopka,[†,§,⊥] and Stefan Wagner[†,⊥]

[†]Department of Nuclear Medicine, University Hospital Münster, Albert-Schweitzer-Campus 1, Building A1, D-48149 Münster, Germany

[‡]European Institute for Molecular Imaging, University of Münster, Mendelstrasse 11, D-48149 Münster, Germany

[§]Interdisciplinary Centre of Clinical Research (IZKF), Albert-Schweitzer-Campus 1, Building D3, D-48149 Münster, Germany

[∥]Siemens Medical Solutions USA, Inc., 6100 Bristol Parkway, Culver City, California 90230, United States

Ⓢ *Supporting Information*
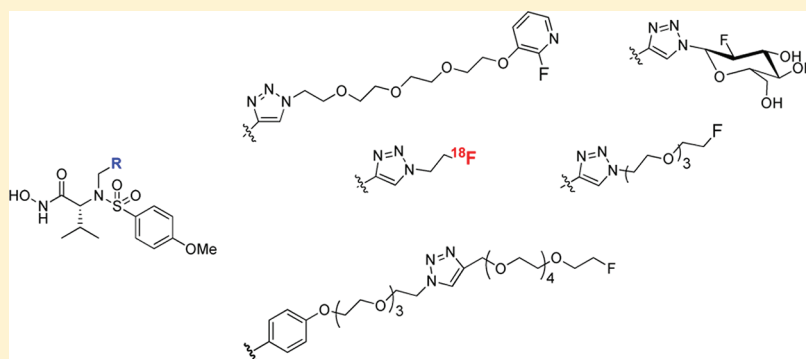
ABSTRACT: In vivo imaging of MMPs is of great (pre)clinical interest and can potentially be realized with modern three-dimensional and noninvasive in vivo molecular imaging techniques such as positron emission tomography (PET). Consequently, MMP inhibitors (MMPIs) radiolabeled with positron emitting nuclides (e.g., ^{18}F) represent a suitable tool for the visualization of activated MMPs with PET. On the basis of our previous work and results regarding radiolabeled and unlabeled derivatives of the nonselective MMPIs, we discovered a new class of fluorinated MMPIs with a triazole-substituted hydroxamate substructure. These novel MMPIs are characterized by an increased hydrophilicity compared with the lead structures and excellent MMP inhibition potencies for MMP-2, MMP-8, MMP-9, and MMP-13 (IC_{50} = 0.006−107 nM). Therefore, one promising fluorinated triazole-substituted hydroxamate (**30b**) was selected and resynthesised as its ^{18}F-labeled version to yield the potential PET radioligand [^{18}F]**30b**. The biodistribution behavior of this novel compound was investigated with small animal PET.

■ INTRODUCTION

In 1962 Jerome Gross and Charles M. Lapière published their studies about the collagenolytic activity in amphibian tissues. They investigated the metamorphosis in tadpole tissues and observed the degradation of collagen by a proteinase that operated at neutral pH and physiological temperature.[1] Six years later, a corresponding enzyme was isolated in its proform from human skin by Eisen et al.[2] The proteinase was initially called interstitial collagenase and was later renamed as matrix metalloproteinase 1 (MMP-1) representing the first member of the matrix metalloproteinase (MMP) enzyme family. Similar to a disintegrin and metalloproteinases (ADAMs) and the ADAMs with a thromospondin motif (ADAMTs), MMPs are a subfamily of the ubiquitously expressed metzincins enzyme superfamily.[3−5] MMPs are multidomain Zn^{2+}-dependent

endopeptidases with a catalytic domain containing two Zn^{2+} and two or three Ca^{2+} ions. The Ca^{2+} ions and one of the Zn^{2+} ions are called structural and are responsible for the stabilization of the domain structure.[6−8] The second Zn^{2+} ion participates in the catalytic process and is located directly in the active site of MMPs. It is coordinated by three histidine residues that are part of the Zn^{2+}-binding consensus sequence HExxHxxGxxH (where x represents a variable amino acid) which is characteristic for proteolytically active metzincins.[9] To date, 23 members of the human MMP family are described that are in the majority of cases excreted as inactive proenzymes characterized by an N-terminal prodomain that shields the

catalytic site from potential substrate molecules. After activation, namely, delocalization of the prodomain, via the so-called cysteine-switch mechanism, MMPs normally possess a broad substrate specificity.[10−12] They degrade on the one hand extracellular matrix (ECM) and basement membrane (BM) proteins and are on the other hand involved in the processing of nonconventional substrates such as cytokines, chemokines, growth factors, serine proteinase inhibitors, cell receptors, and other MMPs.[13] According to their substrate recognition and cleavage mechanism, MMPs can be grouped in collagenases, gelatinases, stromelysins, matrilysins, membrane-associated MMPs, and MMPs with no group designation.[12] MMPs are inhibited and regulated by the common protease inhibitor α_2-macroglobulin, the angiogenesis inhibitor thrombospondin 1 (TSP-1), and the four tissue inhibitors of metalloproteinases (TIMPs).[14] The enzymes are involved in physiological processes such as wound healing,[15] ovulation,[16] muscle homeostasis,[17] bone remodeling,[18] apoptosis,[19] and neurogenesis.[20] In contrast, overexpression and overactivity of MMPs are observed in pathological situations including cancer,[21] rheumatoid arthritis,[22] osteoarthritis,[23] multiple sclerosis, chronic obstructive pulmonary disease,[24] and cardiovascular disease.[25]

Consequently, the molecular imaging of activated MMPs in vivo, preferably with noninvasive approaches in the field of nuclear medicine such as positron emission tomography (PET) and single photon emission computed tomography (SPECT) as well as the optical techniques fluorescence reflectance imaging (FRI) and fluorescence mediated tomography (FMT), is of great (pre)clinical interest because it would represent a powerful tool for the diagnosis and therapy control of MMP associated diseases. A potential approach to achieve this aim is the application of radiolabeled or fluorescence dye-labeled MMP inhibitors (MMPIs) functioning as molecular imaging probes for the visualization of activated MMPs.[26]

In this context two slightly different concepts are followed in our group:

(1) The first strategy is aimed at the specific imaging of discrete subclasses of MMPs. In this case we utilize a pyrimidine-2,4,6-trione (barbiturate) derivative (RO 28-2653) as lead structure for labeled analogues. This compound is described as an MMPI selective for the gelatinases (MMP-2, MMP-9), neutrophil collagenase (MMP-8), and two of the membrane-associated MMPs (MMP-14, MMP-16).[27] Different labeled analogues of this lead structure were synthesized and evaluated partly in vitro and in vivo. Representative barbiturate-based MMPIs were labeled with the γ-emitters ^{125}I and the SPECT-compatible ^{123}I, with the positron emitting [124]I, ^{18}F, and ^{68}Ga and with the fluorescence cyanine dye Cy5.5, resulting in a series of tracers with fine-tuned pharmacokinetics for different imaging modalities.[28−32]

(2) The second approach is based on the development of labeled small-molecule non-peptide MMPIs bearing broad-spectrum inhibition potency without explicit specificity for MMP-subgroups. Here, the hydroxamate-based MMPIs **1a** (CGS 27023A) and **1b** (CGS 25966) were chosen as lead compounds for the design of labeled derivatives (Figure 1). In contrast to the barbiturate analogues, chelating the Zn^{2+} ion of the enzyme active site in a tridentate manner, the CGS analogues coordinate to the Zn^{2+} ion in a bidentate mode using the hydroxamate moiety.[33−35] In addition to the Cy5.5-labeled photoprobe **1b** that shows specific MMP binding in vitro and ex vivo,[36] the ^{123}I-labeled hydroxamate [^{123}I]**1c** (HO[^{123}I]I-
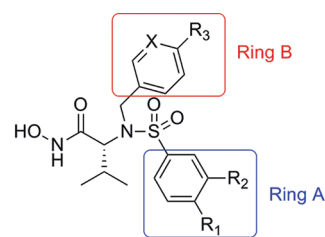
CGS 27023A, **1a**	X: N,	R_1: OCH_3,	R_2: H,	R_3: H
CGS 25966, **1b**	X: CH,	R_1: OCH_3,	R_2: H,	R_3: H
HO-[^{123}I]-CGS 27023A, [^{123}I]**1c**	X: N,	R_1: OH,	R_2: [123]I,	R_3: H
[^{18}F]FEtO-CGS 27023A, [^{18}F]**1d**	X: N,	R_1: OCH_2CH_2[18]F,	R_2: H,	R_3: H
[^{18}F]FEtO-CGS 25966, [^{18}F]**1e**	X: CH,	R_1: OCH_2CH_2[18]F,	R_2: H,	R_3: H
[^{18}F]F-CGS 27023A, [^{18}F]**1f**	X: N,	R_1: OCH_3,	R_2: H,	R_3: [18]F

Figure 1. Lead structures **1a** and **1b** and a selection of radiolabeled analogues.

CGS 27023A) was synthesized and successfully used for specific scintigraphic imaging of MMP activity in the arterial wall of mice in vivo.[37,38] In our subsequent work we focused on the development of a second radiotracer generation characterized by the introduction of the most prominent positron emitter [18]F. Three different analogues ([^{18}F]**1d** ([^{18}F]FEtO-CGS 27023A), [^{18}F]**1e** ([^{18}F]FEtO-CGS 25966), and [^{18}F]**1f** ([^{18}F]F-CGS 27023A)) were radiosynthesized and evaluated in vitro and in vivo.[39−42]

The most promising and accessible candidate [^{18}F]**1e** that represents a hydrophobic member of the series shown in Figure 1 (calculated $\log D$ (clogD) of 4.03; experimental $\log D$ (logD(exp)) of 2.02) was selected for a good manufacturing practices (GMP) compliant fully automated radiosynthesis[43] aiming at first-in-man studies.

To further improve the pharmacokinetics of these hydroxamate-based radiotracers, we aimed to shift the main clearance route from the hepatobiliary system to the kidneys by increasing the hydrophilicity of the new radiotracer class compared to [^{18}F]**1e**.[44] A faster excretion of radiotracer that is not specifically bound to the target tissue results in a desired high signal-to-noise ratio of detected target tissues within a shorter time frame. Therefore, a new class of MMPIs was developed that consists of additional typical hydrophilic moieties,[45−48] such as minipolyethylene glycol (mini-PEG) units and/or triazole subcores, at ring B (Figure 1) or that contains these hydrophilic structural elements instead of ring B. Ring B was chosen for these modifications because this residue is located in the S_2' enzyme pocket that is solvent-exposed and should tolerate limited structural variations.[49] The work presented here describes the (radio)synthesis and in vitro and first in vivo evaluation of a new class of triazole-substituted hydroxamate-based MMPIs displaying remarkable in vitro properties with elevated inhibition potencies and moderate to high hydrophilicities, respectively.

■ RESULTS AND DISCUSSION

Chemistry. To evaluate the MMP inhibition potencies of the new mini-PEG and/or triazole-substituted hydroxamates, the corresponding nonradioactive fluorinated target compounds were synthesized and tested by in vitro fluorogenic MMP assays.

Building blocks used for the synthesis of the MMPIs are represented by the mini-PEG alkyne derivatives **7** and **8** (Scheme 1). Monosubstitution of tetraethylene glycol with

Scheme 1. Syntheses of the Mini-PEG Compounds 7 and 8[a]
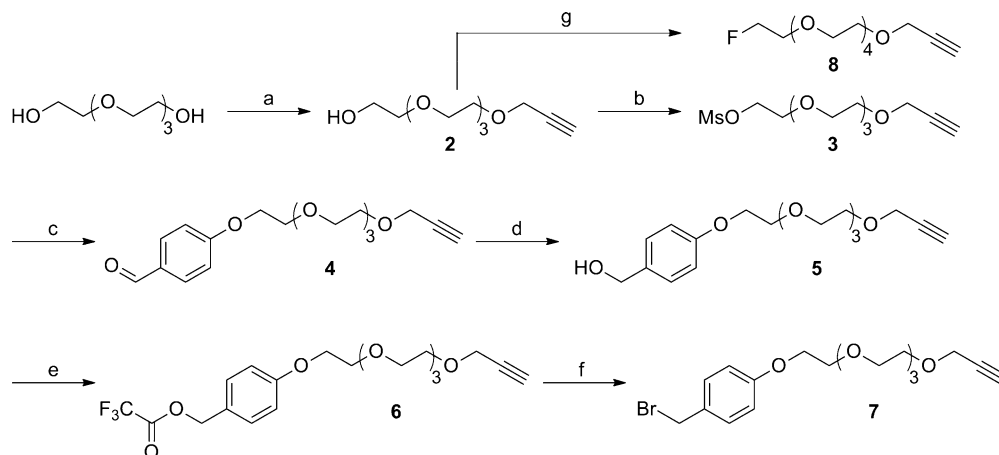
[a]Reaction conditions: (a) propargyl bromide, NaH, THF (41%); (b) MsCl, Et₃N, CH₂Cl₂ (93%); (c) 4-hydroxybenzaldehyde, Cs₂CO₃, DMF (59%); (d) NaBH₄, MeOH (93%); (e) (TFA)₂O, THF (100%); (f) LiBr, THF (100%); (g) 2-fluoroethyl 4-methylbenzenesulfonate,[40] NaH, THF (90%).

Scheme 2. Syntheses of the MMPIs 16a−c[a]
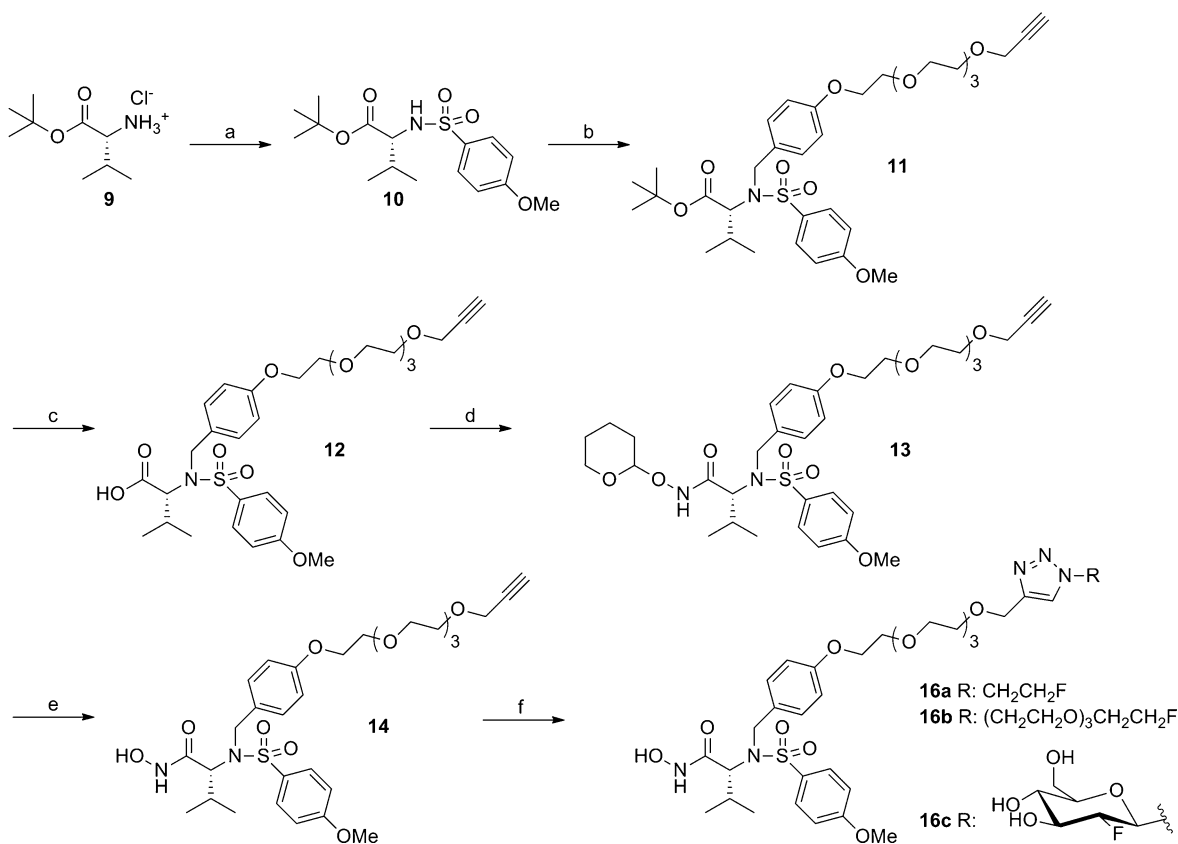
[a]Reaction conditions: (a) 4-methoxybenzene-1-sulfonyl chloride, pyridine (75%); (b) K₂CO₃, DMF, **7** (79%); (c) HCl (gas), CH₂Cl₂ (95%); (d) *O*-(tetrahydro-2*H*-pyran-2-yl)hydroxylamine, EDC, NMM, HOBT, DMF (84%); (e) 4 N HCl in dioxane, methanol/dioxane, 1:1 (89%); (f) CuSO₄·5H₂O, sodium ascorbate, DMF, H₂O, 1-azido-2-fluoroethane (**15a**),[51] 1-azido-2-(2-(2-(2-fluoroethoxy)ethoxy)ethoxy)ethane (**15b**)[30] or 2-deoxy-2-fluoro-*β*-glucopyranosylazide (**15c**)[52] (**16a**, 21%; **16b**, 27%; **16c**, 6%).

propargyl bromide and subsequent mesylation gave the PEGylated alkyne **3**. Nucleophilic substitution of the mesyl moiety with 4-hydroxybenzaldehyde and reduction with sodium borohydride yielded the PEGylated benzyl alcohol **5**, which was converted to the benzyl bromide **7** in two steps. Compound **7** was obtained in overall chemical yield of 21%.

Derivative **8** was obtained with a chemical yield of 37% over both steps by nucleophilic substitution of the monosubstituted mini-PEG alkyne intermediate **2** with 2-fluoroethyl 4-tosylate[40] using sodium hydride.

The synthetic strategy of the **1b** based derivatives **16a−c** with mini-PEG and triazole units is depicted in Scheme 2. The
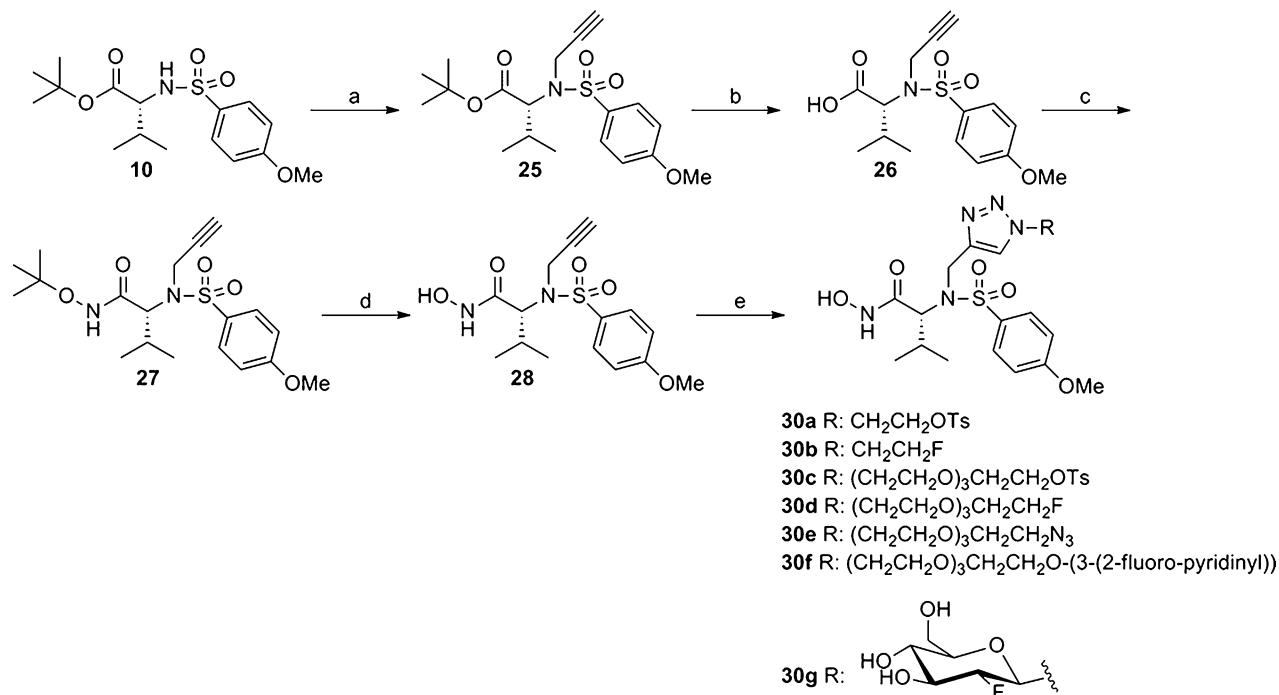
Scheme 3. Synthesis of the MMPI 24[a]
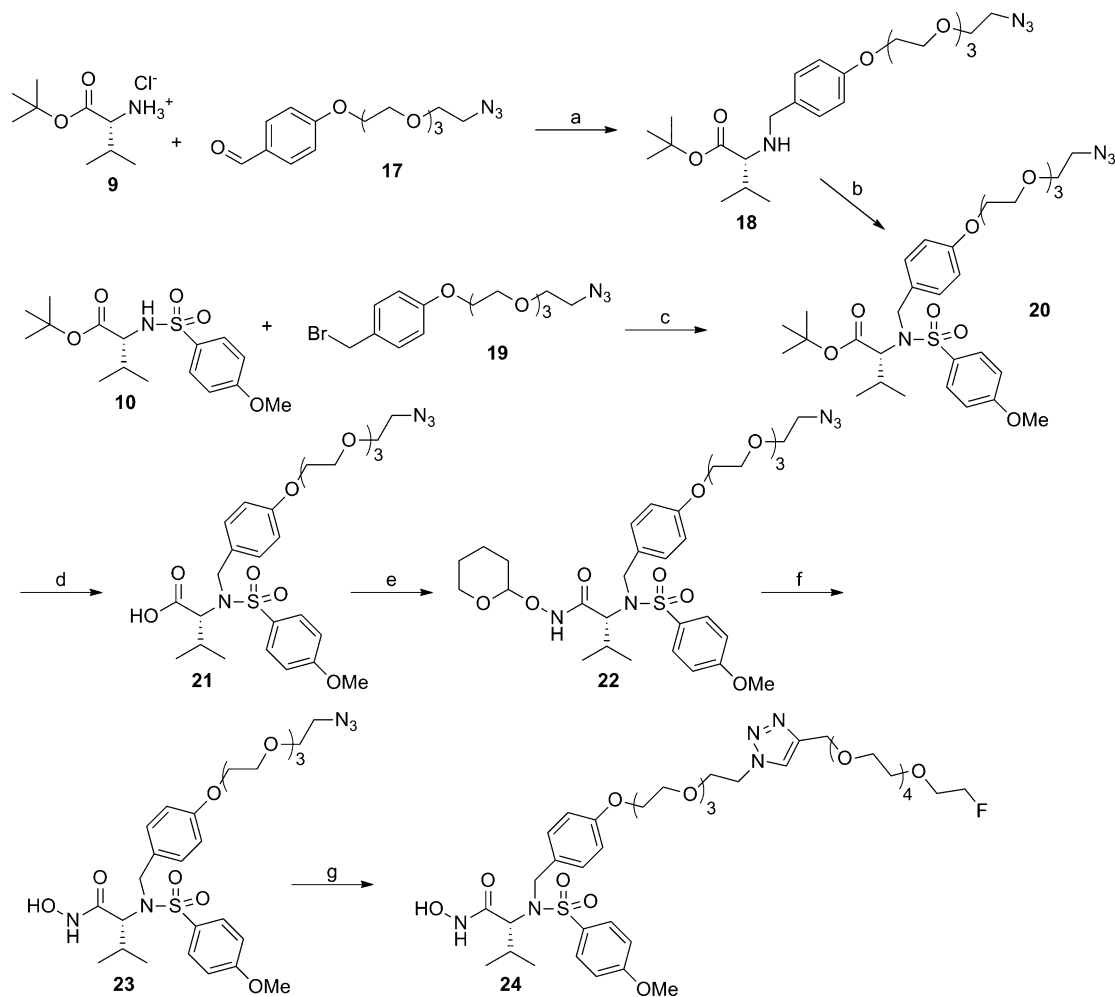
[a]Reaction conditions: (a) NaBH(OAc)$_3$, C$_2$H$_4$Cl$_2$ (90%); (b) 4-methoxybenzene-1-sulfonyl chloride, pyridine (92%); (c) K$_2$CO$_3$, DMF, 7 (66%); (d) HCl (gas), CH$_2$Cl$_2$ (73%); (e) O-THP hydroxylamine, EDC, NMM, HOBT, DMF (92%); (f) 4 N HCl in dioxane, dioxane/MeOH 1:1 (86%); (g) CuSO$_4$·5H$_2$O, sodium ascorbate, DMF, H$_2$O, 8 (6%).

sulfonamide **10** was derived from the commercially available *tert*-butyl ester of D-valine hydrochloride **9** and 4-methoxybenzene-1-sulfonyl chloride in the presence of pyridine. N-Alkylation of **10** with benzyl bromide **7** gave the carboxylic acid ester **11**, which was transformed to the carboxylic acid **12** using gaseous hydrochloric acid in dichloromethane. Conversion of **12** into the corresponding hydroxamic acid ester **13** was achieved by O-THP hydroxylamine, EDC, HOBT, and NMM in DMF. Cleavage of the THP protecting group was performed in a hydrochloric acid containing dioxane/methanol mixture, yielding the alkyne key intermediate **14**. Copper(I) catalyzed Huisgen 1,3-dipolar cycloadditions with different fluorinated azide building blocks (**15a–c**) were employed,[50] providing the 1,2,3-triazole substituted, mini-PEGylated and fluorinated hydroxamic acids **16a–c** with overall chemical yields of 9% for **16a**, 11% for **16b**, and 3% for **16c**.

The azido key intermediate **23** was previously synthesized according to a literature procedure published by our group starting from the sulfonamide **10** and the benzyl bromide **19** (Scheme 3).[36] This synthetic approach was improved in this work because an alternative and shorter synthesis sequence utilizing the azidobenzaldehyde **17** instead of **19** as mini-PEG building block was developed (Scheme 3). Compared to the

synthesis of **19**, the preparation of **17** saved at least three reaction steps.[36] Starting from the *tert*-butyl ester of D-valine **9** and the benzaldehyde **17**, reductive amination with sodium triacetoxyborohydride in dichloroethane provided the N-benzylated D-valine *tert*-butyl ester **18**. Substitution reaction with 4-methoxybenzene-1-sulfonyl chloride in pyridine at 60 °C gave the carboxylic acid ester **20**. After acidic removal of the ester protective group, conversion of the corresponding carboxylic acid **21** into the THP-protected hydroxamic acid ester **22**, and cleavage of the THP protecting group with HCl in dioxane, the key intermediate **23** was obtained in 48% overall yield. Copper(I) catalyzed click reaction with the mini-PEGylated fluoroalkyne **8** provided the double mini-PEGylated 1,2,3-triazole substituted hydroxamic acid **24**.

Compared to the lead structures, hydroxamates **16a–c** and **24** are characterized by the additionally introduced mini-PEG and 1,2,3-triazole units. An advanced approach for the modification of the pharmacokinetics of the lead structure deals with the replacement of ring B by a 1,2,3-triazole unit (Figure 1). The 1,2,3-triazole ring system is endowed with unique chemical and biological stability. In general 1,4-disubstituted 1,2,3-triazoles are putatively metabolically inert and contain H-bond acceptor sites capable of replacing the H-

Scheme 4. Syntheses of the MMPIs 30a−h[a]

30a R: CH$_2$CH$_2$OTs
30b R: CH$_2$CH$_2$F
30c R: (CH$_2$CH$_2$O)$_3$CH$_2$CH$_2$OTs
30d R: (CH$_2$CH$_2$O)$_3$CH$_2$CH$_2$F
30e R: (CH$_2$CH$_2$O)$_3$CH$_2$CH$_2$N$_3$
30f R: (CH$_2$CH$_2$O)$_3$CH$_2$CH$_2$O-(3-(2-fluoro-pyridinyl))

30g R:

[a]Reaction conditions: (a) propargyl bromide, K$_2$CO$_3$, DMF (100%); (b) HCl (gas), CH$_2$Cl$_2$ (99%); (c) t-BuONH$_2$, EDC, NMM, HOBT, CH$_2$Cl$_2$ (88%); (d) HCl (gas), C$_2$H$_4$Cl$_2$ (50%); (e) CuSO$_4$·5H$_2$O, sodium ascorbate, DMF, H$_2$O, 2-azidoethyl 4-methylbenzenesulfonate (29a),[57] 15a,[51] 2-(2-(2-(2-azidoethoxy)ethoxy)ethoxy)ethyl 4-methylbenzene-sulfonate (29b),[30] 15b,[30] 1-azido-2-(2-(2-(2-azidoethoxy)ethoxy)ethoxy)ethane (29c),[36] side product (2R,2'S)-2,2'-(((1,1'-(((oxy-bis(ethane-1,2-diyl))bis(oxy))bis(ethane-1,2-diyl))bis(1H-1,2,3-triazole-1,4-diyl))bis-(methylene))bis(((4-methoxyphenyl)sulfonyl)azanediyl))bis(N-hydroxy-3-methylbutanamide) (30h) was isolated from the reaction with 28, 3-(2-(2-(2-(2-azidoethoxy)ethoxy)ethoxy)ethoxy)-2-fluoropyridine (29d),[31] or 15c[52] (30a, 88%; 30b, 31%; 30c, 73%; 30d, 53%; 30e, 37%; 30f, 18%; 30g, 22%).

Table 1. MMP Inhibition Potencies, clogD, and logD(exp) of Novel Hydroxamic Acids

| compd	IC$_{50}$ (nM)[a]				clogD[b]	logD(exp)
	MMP-2	MMP-8	MMP-9	MMP-13		
1a[41]	3 ± 1	2 ± 0.4	6 ± 3	34 ± 12	2.30	
1b[35]	11[d]	23[d]	27[d]		3.81	
1e[41]	4 ± 3	2 ± 1	50 ± 27	11 ± 0.3	4.03	2.02 ± 0.03
14	0.35 ± 0.1	0.11 ± 0.01	0.37 ± 0.03	0.09 ± 0.03	2.86	
16a	2 ± 1	0.2 ± 0.08	0.6 ± 0.2	6 ± 3	2.09	
16b	4 ± 0.5	5 ± 0.8	5 ± 1	4 ± 1	2.09	
16c	30 ± 10	58 ± 6	43 ± 3	18 ± 2	1.15	
24	4 ± 2	3 ± 2	3 ± 0.3	1 ± 0.2	0.85	
28	5 ± 1	14 ± 2	2 ± 0.4	10 ± 3	2.60	
30a	107 ± 42	8 ± 0.7	7 ± 0.2	5 ± 0.02	2.58	
30b	0.13 ± 0.07	0.02 ± 0.004	0.03 ± 0.003	0.006 ± 0.003	1.53	0.60 ± 0.01[c]
30c	0.07 ± 0.03	0.03 ± 0.001	0.06 ± 0.02	0.02 ± 0.0002	1.87	
30d	0.1 ± 0.03	0.04 ± 0.006	0.05 ± 0.007	0.04 ± 0.007	0.65	
30e	1.2 ± 0.1	9 ± 1	0.9 ± 0.05	6 ± 1	0.77	
30f	3 ± 0.5	5 ± 0.7	4 ± 0.9	1 ± 0.3	1.37	
30g	0.2 ± 0.09	0.5 ± 0.2	0.6 ± 0.2	0.5 ± 0.03	0.58	
30h	>100 μM	>100 μM	>100 μM	>100 μM	1.76	

[a]Values are the mean ± SD of three experiments. [b]clogD values were calculated by ACD/Chemsketch, version ACD/Labs 6.00 (log D = log P at physiological pH 7.4). [c]log D value was determined for compound [^{18}F]30b. [d]K$_i$ values, where SDs are not denoted.

bond acceptor basicity of a peptide bond.[53−56] The synthetic route to a variety of 1,2,3-triazole substituted and mini-PEGylated hydroxamic acid derivatives is depicted in Scheme 4.

N-Alkylation of the sulfonamide 10 with propargyl bromide under basic conditions, acidic hydrolysis of the ester 25 with gaseous hydrochloric acid, and conversion of the carboxylic acid 26 with tert-butylhydroxylamine, EDC, HOBT, and NMM gave the hydroxamic acid ester 27. After the cleavage of the tert-butyl group with hydrochloric acid gas in dichloroethane the propargylic hydroxamic acid 28 was obtained with a high overall yield of 44%. Copper(I) catalyzed click reactions of 28 with different azidoalkyl and azido mini-PEGylated compounds

Scheme 5. Radiosynthesis of ^{18}F-Labeled [^{18}F]30b^a
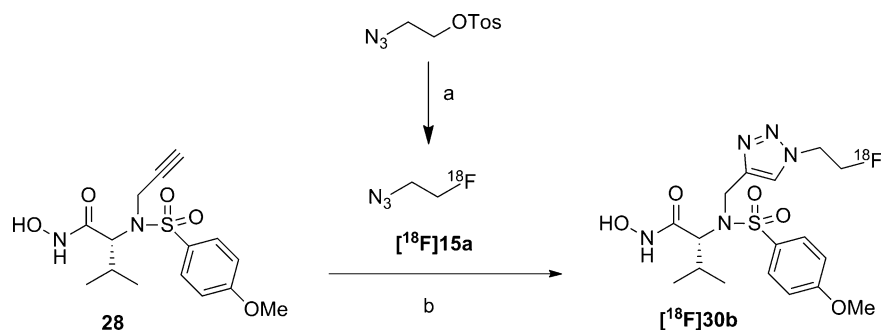
^{a}Reaction conditions: (a) K(K$_{222}$)[^{18}F]F, K$_2$CO$_3$, CH$_3$CN, 110 °C, 100 s (58%); (b) CuSO$_4$·5H$_2$O, sodium ascorbate, DMF, rt, 10 min (55%).

were accomplished with varying yields (18−88%), resulting in a small series of 1,2,3-triazole containing hydrophilic hydroxamic acid derivatives **30a−g**. The 1,2,3-triazoles **30a−g** were prepared using copper(II) sulfate and sodium ascorbate in DMF. A second 1,3-dipolar cycloaddition of compound **30e** with the fluoro-PEG alkyne **8** yielded the desired click reaction product, but purification was impossible because of decomposition of the target compound during the purification procedures.

In summary, a novel class of triazole and/or mini-PEG containing hydroxamate MMPIs were prepared from the alkyne and azido substituted key intermediates **14**, **23**, and **28** by 1,3-dipolar cycloaddition. This reaction strategy yielded fluorinated nonradioactive reference compounds of potential MMP radioligands **16a−c**, **24**, **30b**, **30d**, **30f**, and **30g**, whose MMP inhibiton potencies can be measured by in vitro fluorogenic assays, as well as precursors for ^{18}F-labeling **14**, **23**, **28**, **30a**, and **30c**. Precursors **14**, **23**, and **28** can potentially be ^{18}F-labeled via two-step procedures using radiosynthons, i.e., [^{18}F]15a, [^{18}F]15b, or [^{18}F]15c for the alkyne precursors **14** and **28** and [^{18}F]8 for the azido compound **23**. Nucleophilic substitution of the tosylate precursors **30a** and **30c** with [^{18}F]fluoride can potentially yield the radiofluorinated analogues [^{18}F]30b and [^{18}F]30d in one step.

In Vitro Enzyme Assays and clogD Values. The MMP inhibition potencies of the hydroxamic acids **14**, **16a−c**, **24**, **28**, and **30a−h** against activated MMP-2, -8, -9, and -13 were measured by fluorogenic in vitro inhibition assays following the procedure previously described.[58] The resulting IC$_{50}$ values for the investigated MMPs were compared to those of the parent compounds **1a**, **1b**, and **1e**.

As displayed in Table 1, the new generation of mini-PEG and/or 1,2,3-triazole substituted hydroxamic acids revealed excellent MMP inhibition potencies with IC$_{50}$ values in the nanomolar to picomolar range (0.006−107 nM). In comparison to the potent MMPI **1e** (IC$_{50}$ values of 2−50 nM) the inhibition potencies of **30b−g** were significantly increased with IC$_{50}$ values in the picomolar to low nanomolar range (0.006−5 nM). The 1,2,3-triazole ring appears to play an important role regarding the enzyme binding potencies, and also its position in the molecule seems to be of significance. In particular, compounds **30b−d** and **30g**, with the 1,2,3-triazole moiety positioned close to the hydroxamate group that chelates the Zn^{2+} ion of the enzyme active site in a bidentate manner, show considerably higher inhibition potencies (IC$_{50}$ = 0.006−0.6 nM) than compounds **16a−c** and **24** with a benzyl polyethylene glycol spacer between the backbone of the molecule

and the 1,2,3-triazole unit that still represent potent MMPIs (IC$_{50}$ = 0.2−58 nM).

The aforementioned excellent binding potencies for **30b−d** and **30g** could be due to additional attractive interactions between the hydrophilic triazole nitrogen atoms and the Zn^{2+}ion of the enzyme active site or other functional groups in the enzyme. In contrast, compound **30h** with two triazole substituted hydroxamates linked via a mini-PEG chain (side product of the reaction of **28** with **29c**, formal click product of **30e** and **28**, structure not shown in Scheme 4) was completely inactive in the in vitro assay.

The lead structures based on **1a−b** and **1e** were modified by the introduction of hydrophilic groups such as mini-PEG units and 1,2,3-triazole moieties in combination with fluorinated building blocks. Therefore, an evaluation of the hydrophilic properties of the target compounds is required. Table 1 also displays the calculated log D values (clogD) of the synthesized hydroxamic acids to indicate the changes of the lipophilicities caused by the structural modifications of the lead compounds **1a,b** and the fluorinated analogue **1e**. Compared to **1e** (clogD = 4.03), the new polyethylene glycol and/or 1,2,3-triazole substituted hydroxamic acid derivatives (clogD = 0.58−2.86) show a considerably increased hydrophilicity, as desired.

Additionally, the log D value of the radiofluorinated analogue [^{18}F]30b (see section Radiochemistry) was determined experimentally (logD(exp) = 0.60 ± 0.01). The logD(exp) differs from the clogD (clogD(30b) = 1.53) by 1 unit. Compared to the radiofluorinated analogue [^{18}F]1e (logD (exp) = 2.02 ± 0.03), the triazole substituted hydroxamic acid [^{18}F]30b is approximately 26 times more hydrophilic.

The new MMPI class of mini-PEG and/or 1,2,3-triazole substituted hydroxamates is characterized by at least one major improvement. All new MMPIs showed an increased hydrophilicity compared to the lead structure **1b**. Furthermore backbone triazole substituted MMPIs represented by compounds **30b−d** and **30g** turned out to be the most potent MMPI class developed by our group so far. These results encouraged us to radiosynthesize a representative ^{18}F-labeled isotope for further in vitro and initial in vivo evaluation.

Radiochemistry. Because of the excellent MMPI potency and high hydrophilicity of compound **30b**, this derivative was chosen for the radiosynthesis of its ^{18}F-labeled analogue [^{18}F]30b. For this purpose a semiautomated two-step procedure was developed and optimized (Scheme 5). The preparation of the [^{18}F]fluoroethyl-1,2,3-triazole substituted inhibitor [^{18}F]30b consisted of the nucleophilic radiofluorination of 2-azidoethyl 4-methylbenzenesulfonate and subsequent copper(I) catalyzed cycloaddition with the alkyne precursor **28**.

According to a procedure previously described by Glaser and Årstad, the radiosynthesis of 1-azido-2-[^{18}F]fluoroethane ([^{18}F]**15a**) was achieved.[51] An improvement of the literature procedure could be realized by direct separation of the immediately formed [^{18}F]**15a** from the reaction mixture by destillation. By this we gained a savings of time of at least 15 min compared to the literature procedure. 1-Azido-2-[^{18}F]-fluoroethane could be isolated after 20 min in an average radiochemical yield of 58 ± 4% (decay corrected, $n = 6$). The click labeling was performed outside the automated radio-synthesizer. The optimal reaction conditions proved to be a reaction time of 10 min under stirring at room temperature, using aqueous solutions of copper(II) sulfate pentahydrate (1.4 equiv relative to the alkyne precursor **28**) and sodium ascorbate (1.8 equiv relative to **28**). This reaction step successfully provided the 1,2,3-triazole [^{18}F]**30b** in an average radio-chemical yield of 55 ± 7% (decay corrected, $n = 5$). After purification by semipreparative HPLC and concentration by rotary evaporation and formulation, the two-step radiosynthesis of [^{18}F]**30b** was accomplished with an overall radiochemical yield of 30 ± 3% (decay corrected, $n = 5$) in 110 ± 10 min. [^{18}F]**30b** was isolated in radiochemical purities of >98% with specific activities in the range of 14−57 GBq/μmol at the end of the synthesis. The radioligand was formulated in phosphate-buffered saline (PBS) to determine the log$D$ values and to study its in vitro stability in human serum at 37 °C.

In Vitro Stability. By use of human blood serum, an in vitro stability study was carried out. During long-term incubation for up to 120 min at 37 °C, [^{18}F]**30b** revealed excellent stability. As shown in Figure 2, only the parent compound [^{18}F]**30b** was observed by radio-HPLC. Significant decomposition products or radiometabolites could not be detected. Because of the fact that first in vivo PET experiments were carried out with mice, the blood serum stability measurement of [^{18}F]**30b** was additionally performed in mouse blood serum. Likewise, no significant decomposition of products or radiometabolites were detected (see Supporting Information).

In Vivo Biodistribution Study. Representative coronal whole body images 0−1, 1−5, 5−10, and 90−120 min after tracer injection in C57/BL6 mice are shown in Figure 3.

Overall, [^{18}F]**30b** is cleared quickly and efficiently from the body through hepatic and renal elimination with no significant tracer remaining in nonexcretion organs 90−120 min pi. Immediately upon injection of [^{18}F]**30b** high levels of radioactivity were observed in the liver and the kidneys. While the activity in the kidney decreased ($T_{max} = 30$ s, $T_{1/2} = 13$ min pi) in parallel to the activity in the blood, the liver first showed a further accumulation of [^{18}F]**30b** ($T_{max} = 4$ min, $T_{1/2} = 18$ min pi) before clearance into the gallbladder and finally into the intestine (Figure 4).

Defluorination of the radioligand in vivo potentially impairing image interpretation (indicated by bone uptake of [^{18}F]fluoride ions) was not observed in the entire dynamic imaging study. Furthermore, accumulation of [^{18}F]**30b** in organs/tissues such as the brain, myocardium, lung, and muscles, indicating unspecific binding, was not observed.

Interestingly, in comparison to [^{18}F]**1e**, compound [^{18}F]**30b** does not show any significant difference in the biodistribution characteristics. The overall shapes of the time−activity curves of [^{18}F]**30b** reveal similar radiotracer dynamics as observed in studies using [^{18}F]**1e** (see Figure 4). Only the clearance of [^{18}F]**30b** from kidneys and liver is slightly delayed compared to
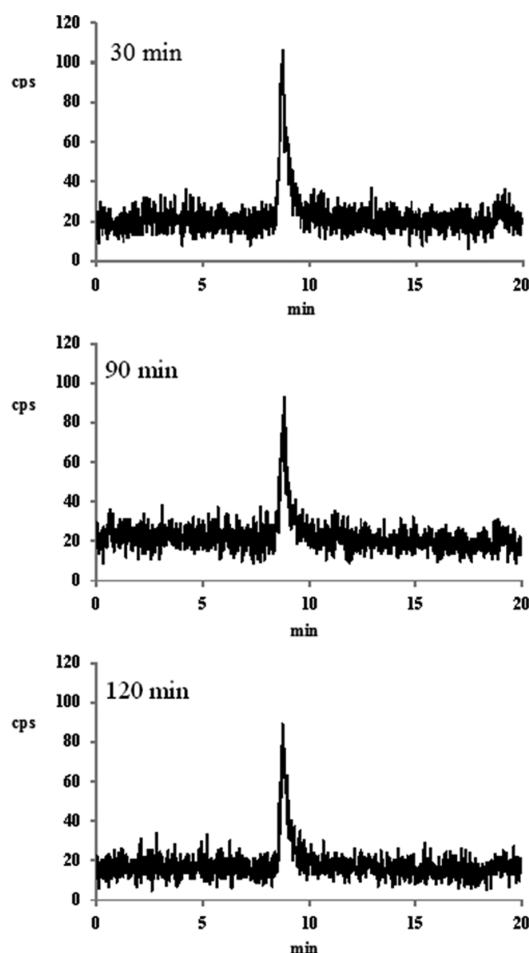

Figure 2. Stability of [^{18}F]**30b** in human blood serum: t_R = 8.70 min; analytical HPLC system A, method A2, starting with 30% CH$_3$CN in water (0.1% TFA) for 15 min, followed by a linear gradient from 30% to 90% CH$_3$CN in water (0.1% TFA) over 3 min, followed by a linear gradient from 90% to 30% CH$_3$CN in water (0.1% TFA) over 2 min with a flow rate of 1 mL·min^{-1} after incubation in human serum in vitro at 37 °C for 30 min (top), 90 min (middle), and 120 min (bottom).

0 − 1 min   1 − 5 min   5 − 10 min   90 − 120 min
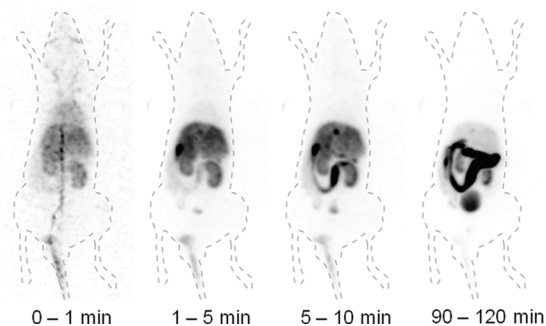
Figure 3. In vivo biodistribution of radioactivity in an adult C57/Bl6 mouse after intravenous injection of [^{18}F]**30b**. Maximum intensity projections of selected time frames after injection demonstrate elimination of radioactivity from the blood primarily via the liver and less pronounced via the kidneys. Bone uptake of [^{18}F]fluoride ions is not observed.

[^{18}F]**1e** (for kidney, $T_{max} = 1.5$ min and $T_{1/2} = 3$ min pi; for liver, $T_{max} = 2.5$ min and $T_{1/2} = 7$ min pi).
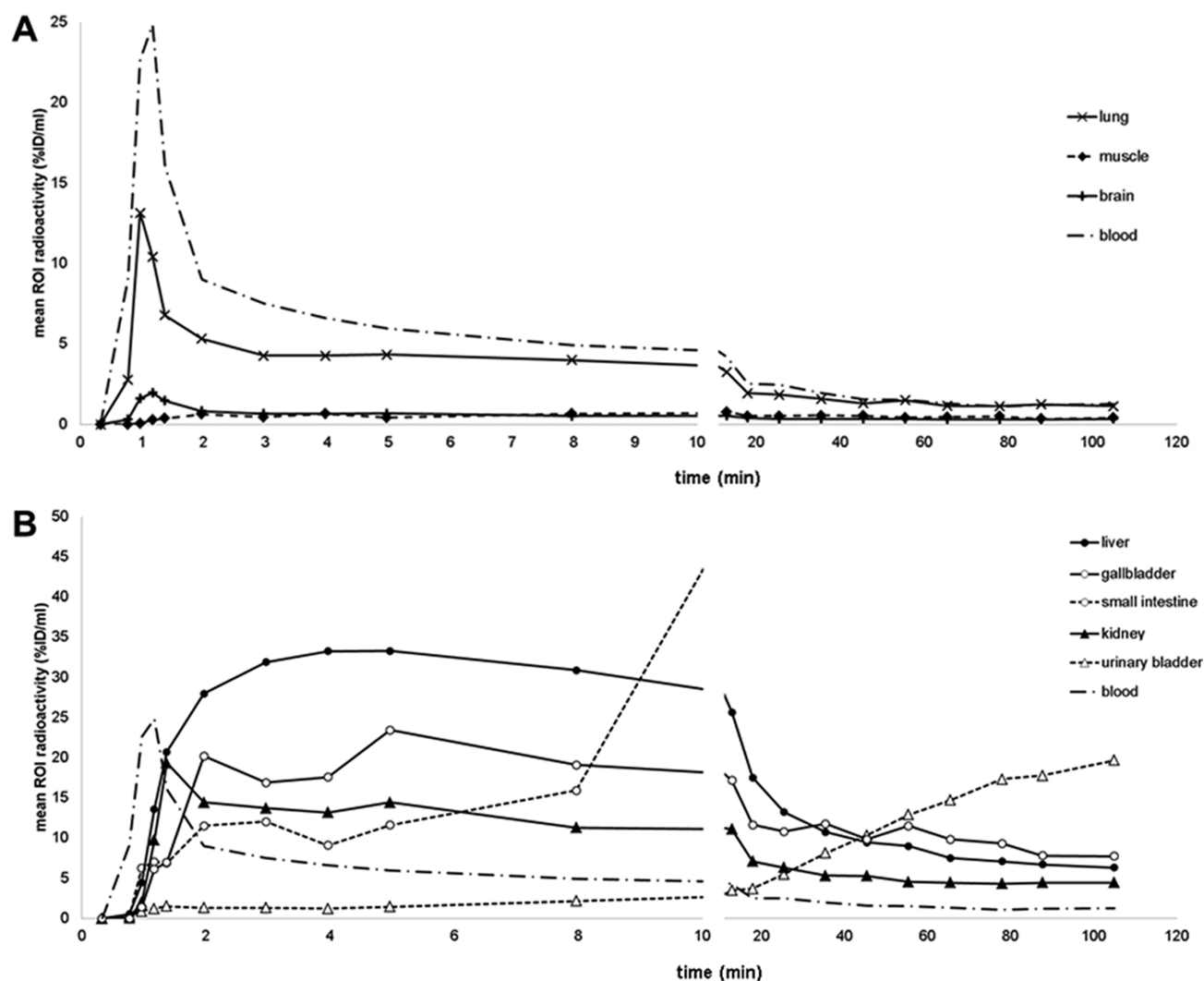
Figure 4. In vivo biodistribution of radioactivity in an adult C57/Bl6 mouse after intravenous injection of [^{18}F]**30b**. Time−activity curves illustrate tracer dynamics in selected regions of interests (ROI). % ID is percentage injected dose.

Obviously, the structural modification of [^{18}F]**1e** directed toward a higher hydrophilicity via the substitution of ring B by a triazole moiety in variant [^{18}F]**30b** did not significantly influence the biodistribution behavior. In future experiments radiolabeled triazole-substituted hydroxamates with an additional hydrophilic subunit (e.g., [^{18}F]**30d** with a mini-PEG chain) will be investigated to examine the influence of an additional shift to higher tracer hydrophilicity on the biodistribution characteristics. Potentially, by the additional introduction of a mini-PEG chain, this structural modification would lead to a radiotracer with the desired increased renal clearance characteristics.

Biostability and Metabolism of [^{18}F]30b. Three 10-month-old female ICR (CD1) wild type mice were examined at 30 min pi to determine the biostability of [^{18}F]**30b**. Representative radio-HPLC traces are shown in Figure 5.

The % ID/g values of the total organs are listed in Table 2 for 30 min time points. The retention time of unchanged [^{18}F]**30b** tracer was between 14.1 and 14.3 min. A total of four metabolites were detected, with retention times of 3.8 min (metabolite 1), 11.1 min (metabolite 2), 13.1 min (metabolite 3), and 16.1 min (metabolite 4).

The muscle % ID/g of [^{18}F]**30b** at 30 min was 0.21% with no other metabolites present. In plasma, at 30 min, the radioactivity was partitioned between 63% (0.29% ID/g) of the parent tracer and 37% (0.17% ID/g) of metabolite 1. No other metabolites were found in plasma. In the liver sample at 30 min, 26% parent (0.78% ID/g) was present while the remaining 74% of activity was distributed between three metabolites, 4% metabolite 1 (0.12% ID/g), 44% metabolite 3 (1.32% ID/g), and 26% metabolite 4 (0.78% ID/g). In the kidney homogenate, the parent tracer was present at higher amounts compared to other tissues at 89% (4.6% ID/g) along with three metabolites: 5% metabolite 1 (0.26% ID/g), 4% metabolite 3 (0.21% ID/g), 2% metabolite 4 (0.1% ID/g). The tracer and the metabolites are predominantly cleared through the kidneys and through urine.

As shown in Table 2, although [^{18}F]**30b** metabolizes to about 37% to a more polar compound in vivo in mice, in plasma no other metabolites were detected. It appears that the tracer clears through urine via kidneys. Though there is some activity remaining in muscle, this might be due to the experimental limitation to exclude blood from muscle.
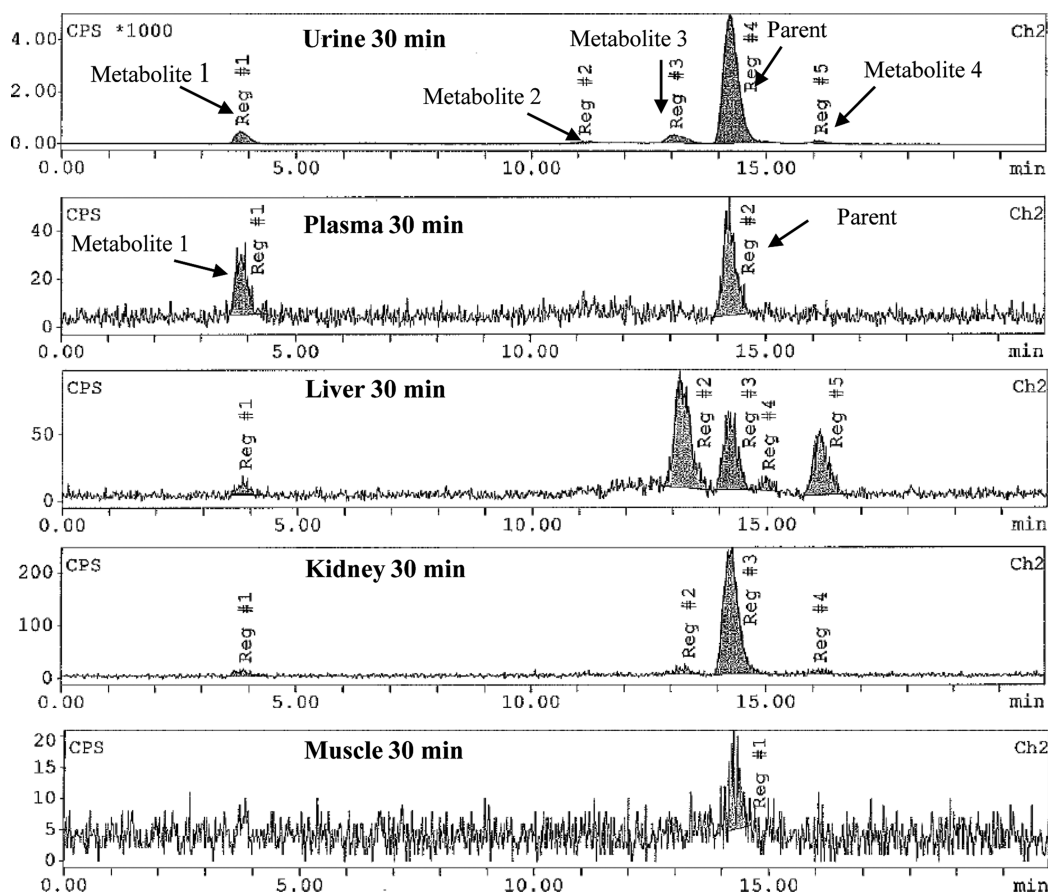
Figure 5. Representative radio-HPLC traces for 30 min pi of the metabolism study of $[^{18}F]$30b. The radiochemical purity of $[^{18}F]$30b was >98% before injection. The samples were analyzed by HPLC, using a γ-detector (Raytest GmbH/Agilent). The HPLC was done on a Phenomenex C18 column (250 mm × 4.6 mm) using a gradient method with acetonitrile and water (both having 0.05% TFA).

Table 2. % ID/g of the Metabolites of $[^{18}F]$30b in Muscle, Kidney, Liver, Plasma, and Urine

	percent injected dose per gram (% ID/g), 30 min pi				
	muscle	kidney	liver	plasma	urine
$[^{18}F]$30b: $t_R \approx 14.2$ min	0.21	4.60	0.78	0.29	27.86
metabolite 1: $t_R \approx 3.8$ min	0.00	0.26	0.12	0.17	2.32
metabolite 2: $t_R \approx 11.1$ min	0.00	0.00	0.00	0.00	0.33
metabolite 3: $t_R \approx 13.1$ min	0.00	0.21	1.32	0.00	2.32
metabolite 4: $t_R \approx 16.1$ min	0.00	0.10	0.78	0.00	0.33

CONCLUSION

On the basis of our previous results with radiolabeled and unlabeled derivatives of the lead MMPIs **1a** and **1b**, the synthesis and in vitro characterization of a new MMPI series of fluorinated triazole-substituted hydroxamates are described. The novel compounds possess moderate to high hydrophilicities with clogD values ranging from 0.58 to 2.86 and represent potent inhibitors of MMP-2, -8, -9, and -13 with IC$_{50}$ values between 0.006 and 107 nM. In particular, inhibitors **30b−d** and **30g** that are characterized by the substitution of the phenyl or pyridyl group by a triazol unit at the ring B position (compare Figure 1) displayed excellent inhibition potencies with IC$_{50}$ values in the picomolar range (0.006−0.6 nM). Compounds **30b−d** and **30g** turned out to be the most potent MMPI class developed so far by our group. The radiosynthesis of the ^{18}F-labeled counterpart $[^{18}F]$30b of the promising derivative **30b** was successfully realized in a two-step procedure with an overall radiochemical yield of 30 ± 3% (decay corrected). The radiofluorinated triazole-substituted hydroxamate MMPI $[^{18}F]$30b showed an excellent serum stability in vitro and a rapid clearance, as shown by in vivo biodistribution studies in wild type mice. Furthermore, undesired unspecific binding of the radiotracer in nonexcretion organs was not observed, and compared to the more lipophilic analogue $[^{18}F]$1e, compound $[^{18}F]$30b does not possesses any significant difference concerning its biodistribution pattern. In any case $[^{18}F]$30b exhibits a promising MMP-targeted radiotracer for the noninvasive PET imaging of activated MMPs in vivo. In future steps compound $[^{18}F]$30b will be evaluated in preclinical PET/CT studies using murine disease models that are characterized by up-regulated levels of activated MMPs (e.g., for atherosclerotic plaques, apolipoprotein E-deficient mice; for tumor, Lewis lung carcinoma bearing mice). In parallel, the radiosynthesis of $[^{18}F]$30d will be established to examine the influence of an additional shift to higher tracer hydrophilicity in vivo.

EXPERIMENTAL SECTION

General. All chemicals, reagents, and solvents for the synthesis of the compounds were analytical grade, purchased from commercial sources, and used without further purification unless otherwise specified. All air- and moisture-sensitive reactions were performed under argon atmosphere. Solvents were purified and dried by literature methods where necessary. The melting points are uncorrected and were determined in capillary tubes on a Stuart Scientific SMP3

capillary melting point apparatus. Column chromatography was performed on Merck silica gel 60 (0.040−0.063 mm). Thin layer chromatography (TLC) was carried out on silica gel coated polyester backed TLC plates (Polygram, SIL G/UV$_{254}$, Macherey-Nagel) using solvent mixtures of cyclohexane (CH), ethyl acetate (EA), and methanol (MeOH). Compounds were visualized by UV light (254 nm). NMR spectra were recorded in CDCl$_3$, CD$_3$OH, or DMSO-d_6 on Bruker ARX300, Bruker DPX300 (^{1}H NMR, 300 MHz; ^{13}C NMR, 75 MHz; ^{19}F NMR, 282 MHz), a Bruker AMX 400 (^{1}H NMR, 400 MHz; ^{13}C NMR, 100 MHz), and Varian Unity Plus 600 (^{1}H NMR, 600 MHz; ^{13}C NMR, 151 MHz) spectrometers. TMS (^{1}H), CDCl$_3$, DMSO-d_6, CD$_3$OH (^{13}C), and CFCl$_3$ (^{19}F) were used as internal standards, and all chemical shifts were recorded in ppm (δ). Exact mass analyses were conducted on a Bruker MicroTof apparatus. The chemical purities of each new nonradioactive compound were ≥95% and assessed by analytical gradient reversed-phase HPLC system A or B (λ = 254 nm). HPLC system A consisted of two Smartline 1000 pumps and a Smartline UV detector 2500 (Herbert Knauer GmbH), a GabiStar γ-detector (Raytest Isotopenmessgeräte GmbH), and a Nucleosil 100-5 C-18 column (250 mm × 4.6 mm). The recorded data were processed by the GINA Star software (Raytest Isotopenmessgeräte GmbH). The HPLC method A1 started with a linear gradient from 10% to 90% CH$_3$CN in water (0.1% TFA) over 9 min, followed by a linear gradient from 90% to 10% CH$_3$CN in water (0.1% TFA) over 6 min, with a flow rate of 1 mL·min^{-1} (unless otherwise specified). HPLC method A2 started with 30% CH$_3$CN in water (0.1% TFA) for 15 min, followed by a linear gradient from 30% to 90% CH$_3$CN in water (0.1% TFA) over 3 min, followed by a linear gradient from 90% to 30% CH$_3$CN in water (0.1% TFA) over 2 min with a flow rate of 1 mL·min^{-1}. HPLC system B consisted of two K-1800 pumps and an S-2500 UV detector (Herbert Knauer GmbH) and a GabiStar γ-detector (Raytest Isotopenmessgeräte GmbH). The recorded data were processed by the ChromGate HPLC software (Herbert Knauer GmbH). HPLC method B1 using a Nucleosil 100-5 C18 column (250 mm × 4.6 mm) started with a linear gradient from 10% to 80% CH$_3$CN in water (0.1% TFA) over 18 min, holding for 20 min and followed by a linear gradient from 80% to 10% CH$_3$CN in water (0.1% TFA) over 2 min, with a flow rate of 1.5 mL·min^{-1}. HPLC method B2 using a ACE 5 AQ column (250 mm × 10 mm) started with a linear gradient from 10% to 80% CH$_3$CN in water (0.1% TFA) over 18 min, holding for 20 min and followed by a linear gradient from 80% to 10% CH$_3$CN in water (0.1% TFA) over 2 min, with a flow rate of 5.5 mL·min^{-1}. N-[(Methoxyphenyl)sulfonyl]-D-valine *tert*-butyl ester (10),[34] 1-azido-2-fluoroethane (15a),[51] 1-azido-2-(2-(2-fluoroethoxy)ethoxy)ethane (15b),[30] 2-deoxy-2-fluoro-β-glucopyranosylazide (15c),[52] 2-azidoethyl 4-methylbenzenesulfonate (29a),[57] 2-(2-(2-(2-azidoethoxy)ethoxy)ethoxy)ethyl 4-methylbenzenesulfonate (29b),[30] 1-azido-2-(2-(2-(2-azidoethoxy)-ethoxy)ethoxy)ethane (29c),[30] 3-(2-(2-(2-(2-azidoethoxy)ethoxy)-ethoxy)ethoxy)-2-fluoropyridine (29d),[31] and 2-fluoroethyl 4-methyl-benzenesulfonate[40] were synthesized following literature procedures. For some long chain compounds ^{13}C NMR signals at $\delta \approx 70$ ppm do have multiple intensities. All animal experiments were conducted in accordance with local institutional guidelines for the care and use of laboratory animals.

Synthesis of MMPI 30b. (R)-*tert*-Butyl 2-(4-Methoxyphenyl-sulfonamido-N-(prop-2-yn-1-yl))-3-methylbutanoate (25). To a solution of (R)-*tert*-butyl 2-(4-methoxyphenylsulfonamido)-3-methyl-butanoate (10) (20.0 g, 58.2 mmol) in DMF (~65 μmol/mL, 900 mL) were added propargyl bromide (80% in toluene, 58.2 mmol, 6.5 mL) and potassium carbonate (582 mmol, 80 g). The resulting suspension was stirred at room temperature for 2 days. The mixture was diluted with water (500 mL) and extracted with EA (3 × 200 mL). The combined organic phases were washed with brine, dried over magnesium sulfate, and the solvent was removed under reduced pressure. The crude product was purified by column chromatography (silica gel; CH/EA, 6:1). The product was obtained as colorless crystals (22.2 g, 58.1 mmol, 100%), mp 79 °C. MS-ES-EM m/z = 404.1507 [(M + Na)$^+$] calcd for C$_{19}$H$_{27}$NO$_5$SNa$^+$: 404.1502.

2-(4-Methoxyphenylsulfonamido-N-(prop-2-yn-1-yl))-3-methylbutanoic Acid (26). A stirred solution of the carboxylic acid ester 25 (22.0 g, 57.67 mmol) in dichloromethane (100 mL) was cooled to 0 °C. Hydrochloric acid gas was bubbled through the solution. TLC was used to monitor the reaction progress (EA). After complete conversion the solvent was removed under reduced pressure to give 26 as a colorless wax (18.6 g, 57.23 mmol, 99%). MS-ES-EM m/z = 348.0877 [(M + Na)$^+$] calcd for C$_{15}$H$_{19}$NO$_5$SNa$^+$: 348.0876.

(R)-N-(*tert*-Butoxy)-2-(4-methoxyphenylsulfonamido-N-(prop-2-yn-1-yl))-3-methylbutanamide (27). To a solution of carboxylic acid 26 (16.3 g, 49.94 mmol) in dichloromethane (0.06 mmol/mL, 830 mL) were added 1-hydroxybenzotriazole hydrate (HOBT, 6.7 g. 49.94 mmol), 4-methylmorpholine (NMM, 27.5 mL, 249.70 mmol), O-*tert*-butylhydroxylamine hydrochloride (18.8 g, 149.82 mmol), and N-((dimethylamino)propyl)-N'-ethylcarbodiimide hydrochloride (EDC, 12.4 g, 64.92 mmol). After being stirred overnight at room temperature, the reaction mixture was diluted with water and extracted with dichloromethane (3 × 200 mL). The combined organic phases were washed with brine, dried over magnesium sulfate, and concentrated to give 27 as a colorless wax (17.4 g, 43.80 mmol, 88%). $[\alpha]_D^{20}$ +107.8 (c 0.98, CHCl$_3$). MS-ES-EM m/z = 419.1614 [(M + Na)$^+$] calcd for C$_{19}$H$_{28}$N$_2$O$_5$SNa$^+$: 419.1611.

(R)-N-Hydroxy-2-(4-methoxyphenylsulfonamido-N-(prop-2-yn-1-yl))-3-methylbutanamide (28). The hydroxamic acid ester 27 (17.3 g, 43.67 mmol) was dissolved in dichloroethane (0.06 mmol/mL, 400 mL) containing 1.0 equiv of ethanol (1.3 mL). The solution was cooled to 0 °C, and hydrochloric acid gas was bubbled through it. TLC was used to monitor the reaction progress (EA). After complete conversion the solvent was removed under reduced pressure. Column chromatography on silica gel (CH/EA, 1:1) yielded 28 as a white solid (7.4 g, 21.75 mmol, 50%), mp 149 °C. MS-ES-EM m/z = 363.0986 [(M + Na)$^+$] calcd for C$_{15}$H$_{20}$N$_2$O$_5$SNa$^+$: 363.0985. HPLC system A, method A1: t_R = 7.32 min (99%).

General Procedure for the Preparation of Triazoles 16a−c, 24, and 30a−h. To a solution of the alkyne compound (0.032−2.0 mmol, 1.0 equiv) in DMF (8 mL/mmol) and H$_2$O (2 mL/mmol) were added CuSO$_4$·5H$_2$O (50 mol %), sodium ascorbate (60 mol %), and the corresponding azide (0.032−2.0 mmol, 1.0−1.2 equiv) in sequence. After being stirred at room temperature, the reaction mixture was diluted with H$_2$O (20 mL) and extracted with EA (3 × 15 mL). The combined organic layers were washed with brine and dried (MgSO$_4$). After evaporation of the solvent, the residue was purified by silica gel column chromatography. Experimental and spectroscopic data of triazoles 16a−c, 24, 30a, 30c−h are listed in the Supporting Information section.

(R)-2-(N-((1-(2-Fluoroethyl)-1H-1,2,3-triazol-4-yl)methyl)-4-methoxyphenylsulfonamido)-N-hydroxy-3-methylbutanamide (30b). 30b was obtained from 28 (340 mg, 1.0 mmol) and 1-azido-2-fluoroethane (15a, 1.0 mmol), prepared from 2-fluoroethyl 4-methylbenzenesulfonate[40] and sodium azide following the literature procedure,[51] after 5 h of stirring at room temperature. Column chromatographic purification (silica gel, EA) gave a white solid (116 mg, 0.31 mmol, 31%), mp 125 °C (dec.). ^{1}H NMR (300 MHz, CDCl$_3$) δ/ppm 10.26 (s, O*H*, 1H), 7.81 (s, CC*H*N, 1H), 7.68 (d, Ar*H*, $^3J_{H,H}$ = 8.6 Hz, 2H), 6.83 (d, Ar*H*, $^3J_{H,H}$ = 8.6 Hz, 2H), 4.99 (d, A**B**, NC*H$_2$*, $^2J_{H,H}$ = 16.6 Hz, 1H), 4.87−4.65 (dm, C*H$_2$*F, $^2J_{H,F}$ = 46.6 Hz, 2H), 4.66−4.53 (dm, NC*H$_2$*CH$_2$F, $^3J_{H,F}$ = 26.2 Hz, 2H), 4.55 (d, **A**B, NC*H$_2$*, $^2J_{H,H}$ = 16.5 Hz, 1H), 3.90 (d, NC*H*, $^3J_{H,H}$ = 10.8 Hz, 1H), 3.78 (s, OC*H$_3$*, 3H), 2.34 (m, C*H*(CH$_3$)$_2$, 1H), 0.83 (d, CH(C*H$_3$*)$_2$, $^3J_{H,H}$ = 6.4 Hz, 3H), 0.57 (d, CH(C*H$_3$*)$_2$, $^3J_{H,H}$ = 6.5 Hz, 3H). ^{13}C NMR (75 MHz, CDCl$_3$) δ/ppm 167.72 (CONH), 163.06 (qArCOCH$_3$), 145.13 (CCHN), 131.07 (qArCSO$_2$), 129.44 (ArCH), 124.85 (CCHN), 114.16 (ArCH), 81.37 (d, CH$_2$F, $^1J_{C,F}$ = 172.9 Hz), 63.62 (NCH), 55.59 (OCH$_3$), 50.52 (d, CH$_2$CH$_2$F, $^2J_{C,F}$ = 20.8 Hz), 39.57 (NCH$_2$), 27.36 (CH(CH$_3$)$_2$), 19.29 (CH(CH$_3$)$_2$), 19.07 (CH(CH$_3$)$_2$). ^{19}F NMR (282 MHz, CDCl$_3$) δ/ppm −222.04 (m, 1F). HRMS-ES-EM m/z = 452.1375 [(M + Na)$^+$] calcd for C$_{17}$H$_{24}$FN$_5$O$_5$SNa$^+$: 452.1374. HPLC system A, method A2: t_R = 8.58 min (100%).

Radiochemistry. General Methods. Radiofluorinations were carried out on a modified PET tracer radiosynthesizer (TRACERLab

Fx$_{FDG}$, GE Healthcare). The recorded data were processed by the TRACERLab Fx software (GE Healthcare). Separation and purification of the radiosynthesized compounds were performed on the following semipreparative radio-HPLC system C (λ = 254 nm): K-500 and K-501 pump, K-2000 UV detector (Herbert Knauer GmbH), NaI(TI) Scintibloc 51 SP51 γ-detector (Crismatec), and an ACE 5 AQ column (250 mm × 10 mm). The recorded data were processed by the GINA Star software (Raytest Isotopenmessgeräte GmbH). Radiochemical purities and specific activities were determined using the analytical radio-HPLC system A and method A2. No-carrier-added aqueous [^{18}F]fluoride was produced on a RDS 111e cyclotron (CTI-Siemens) by irradiation of a 1.2 mL water target using 10 MeV proton beams on 97.0% enriched ^{18}O-water by the ^{18}O(p,n)^{18}F nuclear reaction.

(R)-2-(N-((1-(2-[^{18}F]Fluoroethyl)-1H-1,2,3-triazol-4-yl)-methyl)-4-methoxyphenylsulfonamido)-N-hydroxy-3-methylbutanamide ([^{18}F]30b). In a computer controlled TRACERLab Fx$_{FDG}$ synthesizer aqueous [^{18}F]fluoride ions (0.1−5.5 GBq) from the cyclotron target were passed through an anion exchange resin (Sep-Pak Light Waters Accell Plus QMA cartridge, preconditioned with 5 mL of 1 M K$_2$CO$_3$ and 10 mL of water for injection). [^{18}F]Fluoride ions were eluted from the resin with a mixture of 40 μL of 1 M K$_2$CO$_3$, 200 μL of water for injection, and 800 μL of DNA-grade CH$_3$CN containing 18 mg (48 μmol) of Kryptofix 2.2.2 (K222) in the reactor. Subsequently, the aqueous K(K222) [^{18}F]F solution was carefully evaporated to dryness in vacuo. An amount of 12 μL (14 mg, 60 μmol) of precursor 2-azidoethyl 4-methylbenzenesulfonate[57] in 300 μL of dry DMF was added, and the mixture was heated at 110 °C for 100 s. Meanwhile, the labeled product [^{18}F]15a was distilled from the reactor in a 5 mL flask that contained 400 μL of dry DMF and was cooled to −10 °C. The radiosynthon [^{18}F]15a was collected with a radiochemical yield of 58 ± 4% in 20 min (mean ± SD, decay corrected, n = 6). Then 60 μL of 0.4 M CuSO$_4$·5H$_2$O, 40 μL of water, 6 mg (30 μmol) of sodium ascorbate in 100 μL of water, and 6 mg (17.6 μmol) of alkyne 28 in 100 μL of DMF were added. After 10 min at ambient temperature, the mixture was passed through a Waters Sep-Pak Light cartridge filled with quartz wool. The cartridge was rinsed with DMF (0.2 mL). The eluate was diluted with 500 μL of water, and the resulting mixture was purified by gradient-radio-HPLC system C (flow = 5.5 mL/min; eluents, A, CH$_3$CN/TFA, 1000/1, B, H$_2$O/TFA, 1000/1; isocratic, A/B 18/82 (v/v); λ = 254 nm; column, ACE 5 AQ (250 mm × 10 mm)). The product fraction of compound [^{18}F]30b (retention time t_R([^{18}F]30b) = 37 min) was evaporated to dryness in vacuo and redissolved in 1 mL of 0.9% NaCl/EtOH (9/1 v/v). Product compound [^{18}F]30b was obtained in an overall radiochemical yield of 30 ± 3% (decay-corrected, based on cyclotron-derived [^{18}F]fluoride ions, n = 5) in 110 ± 10 min from the end of radionuclide production. [^{18}F]30b was isolated in radiochemical purities of >98% with specific activities in the range of 14−57 GBq/μmol at the end of the synthesis.

In Vitro Enzyme Inhibition Assays (Table 1). The inhibition potencies of hydroxamic acid derivatives 14, 16a−c, 24, 28, and 30a−h against activated MMP-2, -8, -9, and -13 were assayed using the synthetic fluorogenic substrate (7-methoxycoumarin-4-yl)acetyl-Pro-Leu-Gly-Leu-(3-(2,4-dinitrophenyl)-L-2,3-diaminopropionyl)Ala-Arg-NH$_2$ (R&D Systems) as described previously.[58] Briefly, MMP-2, -8, -9, or -13 (each at 2 nM) and test compounds at varying concentrations (10 pM to 1 mM) in Tris-HCl (50 mM), pH 7.5, containing NaCl (0.2 M), CaCl$_2$ (5 mM), ZnSO$_4$ (20 μM), and 0.05% Brij 35 were preincubated at 37 °C for 30 min. An aliquot of substrate (10 μL of a 50 μM solution) was added to the enzyme−inhibitor mixture (90 μL), and the fluorescence changes were monitored using a Fusion Universal microplate analyzer (Packard Bioscience) with excitation and emission wavelengths of 330 and 390 nm, respectively. Reaction rates were measured from the initial 10 min and plotted as a function of inhibitor concentration. From the resulting inhibition curves, the IC$_{50}$ values were calculated by nonlinear regression analysis using the Grace 5.1.8 software (Linux).

Determination of the Partition Coefficient (log $D_{7.4}$). The lipophilicity of radioligand [^{18}F]30b was assessed by determination of

the water−octanol partition coefficient following a published procedure.[59] In brief, an amount of approximately 20 kBq [^{18}F]30b was mixed with equal amounts (0.5 mL) of PBS (pH 7.4) and 1-octanol, and the resulting biphasic system was mixed vigorously for 1 min at room temperature. The tubes were centrifuged (3000 rpm, 2 min), and three samples of 100 μL of each layer were counted in a γ counter (Wallac Wizard, Perkin-Elmer Life Sciences). The partition coefficient was determined by calculating the ratio cpm(octanol)/cpm(PBS) and expressed as log $D_{7.4}$ (log(cpm$_{octanol}$/cpm$_{PBS}$)). Two independent experiments were performed in triplicate, and data were provided as mean values ± standard deviation.

Stability in Human Serum. The serum stability of radioligand [^{18}F]30b was evaluated by incubation in human serum at 37 °C for up to 120 min. An aliquot of the PBS-formulated ^{18}F-labeled compound (20 μL, 5 MBq) was added to a sample of human serum (200 μL), and the mixture was incubated at 37 °C. Samples of 20 μL each were taken after periods of 10, 20, 30, 60, 90, and 120 min and quenched in methanol/CH$_2$Cl$_2$ (1:1 (v/v), 100 μL) followed by centrifugation for 2 min. The organic layer was analyzed by analytical radio-HPLC (t_R = 8.70 min; analytical HPLC system A, method A2, starting with 30% CH$_3$CN in water (0.1% TFA) for 15 min, followed by a linear gradient from 30% to 90% CH$_3$CN in water (0.1% TFA) over 3 min, followed by a linear gradient from 90% to 30% CH$_3$CN in water (0.1% TFA) over 2 min with a flow rate of 1 mL·min^{-1}).

Biostability and Metabolism Study. Approximately 11.1 MBq [^{18}F]30b (in a maximum volume of 200 μL) was injected into three mice via tail vein injection. The animals were sacrificed at 30 min pi. Whole blood was obtained, weighed, and centrifuged at 3000 rpm (3 min) to isolate plasma. Urine was also collected. The muscle, kidneys, and liver were harvested, weighed, and homogenized in lysis buffer (1% SDS in PBS buffer). An aliquot of each sample (400 μL) was subsequently removed, mixed with 400 μL of acetonitrile and 100 μL of 3% acetic acid in acetonitrile, vigorously mixed, and placed on dry ice for 3 min. After thawing, the samples were centrifuged at 13000 rpm (8 min) to allow for the separation of supernatant from the pellet. The supernatant was then removed and assayed for radioactivity in a PerkinElmer Wizard γ-counter (20 s). A 2 μL aliquot from the dose sample was counted along with the samples and was used to calculate the % ID/g. The samples were analyzed by HPLC, using a γ-detector (Raytest GmbH/Agilent). HPLC was done on a Phenomenex C18 column (250 mm × 4.6 mm) using a gradient method with acetonitrile and water (both having 0.05% TFA).

Animals. Adult C57/BL6 mice (male, 21−24 g) were anesthetized by isoflurane/O$_2$, and one lateral tail vein was cannulated using a 27 Ga needle connected to 15 cm polyethylene catheter tubing. [^{18}F]1e or [^{18}F]30b (250 kBq/g bodyweight) was injected as a bolus (100 μL of compound flushed with 100 μL of saline) via the tail vein, and subsequent PET scanning was performed. Experiments were conducted according to German animal welfare guidelines.

Small Animal PET Scanning. PET experiments were carried out using a submillimeter high resolution (0.7 mm full width at half-maximum) small animal scanner (32 module quadHIDAC, Oxford Positron Systems Ltd., Oxford, U.K.) with uniform spatial resolution (<1 mm) over a large cylindrical field (165 mm diameter, 280 mm axial length).[60]

List-mode data were acquired for 120 min and reconstructed into dynamic time frames using an iterative reconstruction algorithm. Subsequently, the scanning bed was transferred to the computed tomography (CT) scanner (Inveon, Siemens Medical Solutions, U.S.) and a CT acquisition with a spatial resolution of 80 μm was performed for each mouse. Reconstructed image data sets were co-registered based on extrinsic markers attached to the multimodal scanning bed and the image analysis software (Inveon Research Workplace 3.0, Siemens Medical Solutions, USA). Three-dimensional volumes of interest (VOIs) were defined over the respective organs in CT data sets, transferred to the co-registered PET data, and analyzed quantitatively. Regional uptake was calculated as percentage of injected dose by dividing counts per milliliter in the VOI by total counts in the mouse multiplied by 100 (% ID/mL).

ASSOCIATED CONTENT

S **Supporting Information**

Experimental procedures and analytical data for compounds **1**−**8**, **10**−**14**, **18**, **20**−**23** and NMR data of **25**−**28**. This material is available free of charge via the Internet at http://pubs.acs.org.

AUTHOR INFORMATION

Corresponding Author

*Phone: +492518347851. Fax: +498347363. E-mail: hugenber@uni-muenster.de.

Author Contributions

[⊥]Both authors contributed equally to this work and share senior authorship.

Notes

The authors declare no competing financial interest.

ACKNOWLEDGMENTS

ABBREVIATIONS USED

ADAM, a disintegrin and metalloproteinase; ADAMT, a disintegrin and metalloproteinase with a thromospondin motif; BM, basement membrane; CH, cyclohexane; ECM, extracellular matrix; EDC, N'-ethyl-N'-(3-dimethylaminopropyl)carbodiimide hydrochloride; EA, ethyl acetate; EM, exact mass; FMT, fluorescence mediated tomography; FRI, fluorescence reflectance imaging; GMP, good manufacturing practices; HOBT, 1-hydroxybenzotriazole; ICR, imprinting control region; K222, Kryptofix 2.2.2; log D, log P at physiological pH 7.4; MMP, matrix metalloproteinase; MMPI, matrix metalloproteinase inhibitor; NMM, 4-methylmorpholine; PEG, polyethylene glycol; PET, positron emission tomography; pi, postinjection; ROI, region of interest; % ID, percentage injected dose; SD, standard deviation; SPECT, single photon emission computed tomography; THP, tetrahydropyranyl; TIMP, tissue inhibitor of metalloproteinase

REFERENCES

(1) Gross, J.; Lapière, C. M. Collagenolytic activity in amphibian tissues: a tissue culture assay. *Proc. Natl. Acad. Sci. U.S.A.* **1962**, *48*, 1014−1022.

(2) Eisen, A. Z.; Jeffrey, J. J.; Gross, J. Human skin collagenase. Isolation and mechanism of attack on the collagen molecule. *Biochim. Biophys. Acta* **1968**, *151*, 637−645.

(3) White, J. M. ADAMs: modulators of cell−cell and cell−matrix interactions. *Curr. Opin. Cell Biol.* **2003**, *15*, 598−606.

(4) Tang, B. L. ADAMTs: a novel family of extracellular matrix proteases. *Int. J. Biochem. Cell Biol.* **2001**, *33*, 33−44.

(5) Nagase, H.; Woessner, J. F., Jr. Matrix metalloproteinases. *J. Biol. Chem.* **1999**, *274*, 21491−21494.

(6) Stocker, W.; Bode, W. Structural features of a superfamily of zinc-endopeptidases: the metzincins. *Curr. Opin. Struct. Biol.* **1995**, *5*, 383−390.

(7) Dhanaraj, V.; Ye, Q. Z.; Johnson, L. L.; Hupe, D. J.; Ortwine, D. F.; Dunbar, J. B., Jr.; Rubin, J. R.; Pavlovsky, A.; Humblet, C.; Blundell, T. L. X-ray structure of a hydroxamate inhibitor complex of stromelysin catalytic domain and its comparison with members of the zinc metalloproteinase superfamily. *Structure* **1996**, *4*, 375−386.

(8) Borkakoti, N. Structural studies of matrix metalloproteinases. *J. Mol. Med.* **2000**, *78*, 261−268.

(9) Bode, W.; Gomis-Rüth, F. X.; Stöckler, W. Astacins, serralysins, snake venom and matrix metalloproteinases exhibit identical zinc-binding environments (HEXXHXXGXXH and Met-turn) and topologies and should be grouped into a common family, the "metzincins". *FEBS Lett.* **1993**, *331*, 134−140.

(10) Van Wart, H. E.; Birkedal-Hansen, H. The cysteine switch: a principle of regulation of metalloproteinase activity with potential applicability to the entire matrix metalloproteinase gene family. *Proc. Natl. Acad. Sci. U.S.A.* **1990**, *87*, 5578−5582.

(11) Ra, H. J.; Parks, W. C. Control of matrix metalloproteinase catalytic activity. *Matrix Biol.* **2007**, *26*, 587−596.

(12) Zitka, O.; Kukacka, J.; Krizkova, S.; Huska, D.; Adam, V.; Masarik, M.; Prusa, R.; Kizek, R. Matrix metalloproteinases. *Curr. Med. Chem.* **2010**, *17*, 3751−3768.

(13) Butler, G. S.; Overall, C. M. Updated biological roles for matrix metalloproteinases and new "intracellular" substrates revealed by degradomics. *Biochemistry* **2009**, *48*, 10830−10845.

(14) Brew, K.; Nagase, H. The tissue inhibitors of metalloproteinases (TIMPs): an ancient family with structural and functional diversity. *Biochim. Biophys. Acta* **2010**, *1803*, 55−71.

(15) Gill, S. E.; Parks, W. C. Metalloproteinases and their inhibitors: regulators of wound healing. *Int. J. Biochem. Cell Biol.* **2008**, *40*, 1334−1347.

(16) Zhang, X.; Nothnick, W. B. The role and regulation of the uterine matrix metalloproteinase system in menstruating and non-menstruating species. *Front. Biosci.* **2005**, *10*, 353−366.

(17) Carmeli, E.; Moas, M.; Reznick, A. Z.; Coleman, R. Matrix metalloproteinases and skeletal muscle: a brief review. *Muscle Nerve* **2004**, *29*, 191−197.

(18) Krane, S. M.; Inada, M. Matrix metalloproteinases and bone. *Bone* **2008**, *43*, 7−18.

(19) Mathew, S.; Fu, L.; Hasebe, T.; Ishizuya-Oka, A.; Shi, Y. B. Tissue-dependent induction of apoptosis by matrix metalloproteinase stromelysin-3 during amphibian metamorphosis. *Birth Defects Res., Part C* **2010**, *90*, 55−66.

(20) Agrawal, S. M.; Lau, L.; Yong, V. W. MMPs in the central nervous system: where the good guys go bad. *Semin. Cell Dev. Biol.* **2008**, *19*, 42−51.

(21) (a) Fingleton, B. Matrix metalloproteinases: roles in cancer and metastasis. *Front. Biosci.* **2006**, *11*, 479−491. (b) Kessenbrock, K.; Plaks, V.; Werb, Z. Matrix metalloproteinases: regulators of the tumor microenvironment. *Cell* **2010**, *141*, 52−67. (c) Gialeli, C.; Theocharis, A. D.; Karamanos, N. K. Roles of matrix metalloproteinases in cancer progression and their pharmacological targeting. *FEBS J.* **2011**, *278*, 16−27.

(22) Okamoto, H.; Hoshi, D.; Kiire, A.; Yamanaka, H.; Kamatani, N. Molecular targets of rheumatoid arthritis. *Inflamm. Allergy: Drug Targets* **2008**, *7*, 53−66.

(23) Troeberg, L.; Nagase, H. Proteases involved in cartilage matrix degradation in osteoarthritis. *Biochim. Biophys. Acta* **2012**, *1824*, 133−145.

(24) Muroski, M. E.; Roycik, M. D.; Newcomer, R. G.; Van den Steen, P. E.; Opdenakker, G.; Monroe, H. R.; Sahab, Z. J.; Sang, Q. X. Matrix metalloproteinase-9/gelatinase B is a putative therapeutic target of chronic obstructive pulmonary disease and multiple sclerosis. *Curr. Pharm. Biotechnol.* **2008**, *9*, 34−46.

(25) (a) Brauer, P. R. MMPs-role in cardiovascular development and disease. *Front. Biosci.* **2006**, *11*, 447−478. (b) Papazafiropoulou, A.; Tentolouris, N. Matrix metalloproteinases and cardiovascular diseases. *Hippokratia* **2009**, *13*, 76−82.

(26) Wagner, S.; Breyholz, H.-J.; Faust, A.; Höltke, C.; Levkau, B.; Schober, O.; Schäfers, M; Kopka, K. Molecular imaging of matrix

metalloproteinases in vivo using small molecule inhibitors for SPECT and PET. *Curr. Med. Chem.* **2006**, *13*, 2819−2838.

(27) Grams, F.; Brandstetter, H.; D'Alo, S.; Geppert, D.; Krell, H. W.; Leinert, H.; Livi, V.; Menta, E.; Oliva, A.; Zimmermann, G. Pyrimidine-2,4,6-triones: a new effective and selective class of matrix metalloproteinase inhibitors. *Biol. Chem.* **2001**, *382*, 1277−1285.

(28) Breyholz, H.-J.; Schäfers, M.; Wagner, S.; Höltke, C.; Faust, A.; Rabeneck, H.; Levkau, B.; Schober, O.; Kopka, K. C-5-disubstituted barbiturates as potential molecular probes for noninvasive matrix metalloproteinase imaging. *J. Med. Chem.* **2005**, *48*, 3400−3409.

(29) Kopka, K.; Breyholz, H.-J.; Wagner, S.; Brandau, W.; Hermann, S.; Schober, O.; Levkau, B.; Bremer, C.; Schäfers, M. Radioiodinated pyrimidine-2,4,6-triones as model probes for the in vivo molecular imaging of activated MMPs. *J. Labelled Compd. Radiopharm.* **2007**, *50*, S397.

(30) Breyholz, H.-J.; Wagner, S.; Faust, A.; Riemann, B.; Höltke, C.; Hermann, S.; Schober, O.; Schäfers, M.; Kopka, K. Radiofluorinated pyrimidine-2,4,6-triones as molecular probes for noninvasive MMP-targeted imaging. *ChemMedChem.* **2010**, *5*, 777−789.

(31) Schrigten, D.; Breyholz, H.-J.; Wagner, S.; Hermann, S.; Schober, O.; Schäfers, M.; Haufe, G.; Kopka, K. A new generation of radiofluorinated pyrimidine-2,4,6-triones as MMP-targeted radiotracers for positron emission tomography. *J. Med. Chem.* **2012**, *55*, 223−232.

(32) Faust, A.; Waschkau, B.; Waldeck, J.; Höltke, C.; Breyholz, H.-J.; Wagner, S.; Kopka, K.; Schober, O.; Heindel, W.; Schäfers, M.; Bremer, C. Synthesis and evaluation of a novel photoprobe for imaging matrix metalloproteinases. *Bioconjugate Chem.* **2008**, *19*, 1001−1008.

(33) Brandstetter, H.; Grams, F.; Glitz, D.; Lang, A.; Huber, R.; Bode, W.; Krell, H. W.; Engh, R. A. The 1.8-Å crystal structure of a matrix metalloproteinase-8 barbiturate inhibitor complex reveals a previously unobserved mechanism for collagenase substrate recognition. *J. Biol. Chem.* **2001**, *276*, 17405−17412.

(34) MacPherson, L. J.; Bayburt, E. K.; Capparelli, M. P.; Carroll, B. J.; Goldstein, R.; Justice, M. R.; Zhu, L.; Hu, S. I.; Melton, R. A.; Fryer, L.; Goldberg, R. L.; Doughty, J. R.; Spirito, S.; Blancuzzi, V.; Wilson, D.; O'Byrne, E. M.; Ganu, V.; Parker, D. T. Discovery of CGS 27023A, a non-peptidic, potent, and orally active stromelysin inhibitor that blocks cartilage degradation in rabbits. *J. Med. Chem.* **1997**, *40*, 2525−2532.

(35) Scozzafava, A.; Supuran, C. T. Carbonic anhydrase and matrix metalloproteinase inhibitors: sulfonylated amino acid hydroxamates with MMP inhibitory properties act as efficient inhibitors of CA isozymes I, II, and IV, and N-hydroxysulfonamides inhibit both these zinc enzymes. *J. Med. Chem.* **2000**, *43*, 3677−3687.

(36) Faust, A.; Waschkau, B.; Waldeck, J.; Höltke, C.; Breyholz, H.-J.; Wagner, S.; Kopka, K.; Schober, O.; Heindel, W.; Schäfers, M.; Bremer, C. Synthesis and evaluation of a novel hydroxamate based fluorescent photoprobe for imaging matrix metalloproteinases. *Bioconjugate Chem.* **2009**, *20*, 904−912.

(37) Kopka, K.; Breyholz, H.-J.; Wagner, S.; Law, M. P.; Riemann, B.; Schröer, S.; Trub, M.; Guilbert, B.; Levkau, B.; Schober, O.; Schäfers, M. Synthesis and preliminary biological evaluation of new radioiodinated MMP inhibitors for imaging MMP activity in vivo. *Nucl. Med. Biol.* **2004**, *31*, 257−267.

(38) Schäfers, M.; Riemann, B.; Kopka, K.; Breyholz, H.-J.; Wagner, S.; Schäfers, K. P.; Law, M .P.; Schober, O.; Levkau, B. Scintigraphic imaging of matrix metalloproteinase activity in the arterial wall in vivo. *Circulation* **2004**, *109*, 2554−2559.

(39) Breyholz, H.-J.; Wagner, S.; Levkau, B.; Schober, O.; Schäfers, M.; Kopka, K. A ^{18}F-radiolabelled analogue of CGS 27023A for assessment of matrix-metalloproteinase activity in vivo. *Q. J. Nucl. Med. Mol. Imaging* **2007**, *51*, 24−32.

(40) Wagner, S.; Breyholz, H.-J.; Law, M. P.; Faust, A.; Höltke, C.; Schröer, S.; Haufe, G.; Levkau, B.; Schober, O.; Schäfers, M.; Kopka, K. Novel fluorinated derivatives of the broad-spectrum MMP inhibitors N-hydroxy-2(R)-{[(4-methoxyphenyl)sulfonyl](benzyl)-and (3-picolyl)-amino}-3-methyl-butanamide as potential tools for

the molecular imaging of activated MMPs with PET. *J. Med. Chem.* **2007**, *50*, 5752−5764.

(41) Wagner, S.; Breyholz, H.-J.; Höltke, C.; Faust, A.; Schober, O; Schäfers, M.; Kopka, K. A new ^{18}F-labelled derivative of the MMP inhibitor CGS 27023A for PET: radiosynthesis and initial small-animal PET studies. *Appl. Radiat. Isot.* **2009**, *67*, 606−610.

(42) Schäfers, M.; Schober, O.; Hermann, S. Matrix-metalloproteinases as imaging targets for inflammatory activity in atherosclerotic plaques. *J. Nucl. Med.* **2010**, *51*, 663−666.

(43) Wagner, S.; Faust, A.; Breyholz, H.-J.; Schober, O.; Schäfers, M.; Kopka, K. The MMP inhibitor (R)-2-(N-benzyl-4-(2-[18F]-fluoroethoxy)phenylsulfonamido)-N-hydroxy-3-methylbutanamide: improved precursor synthesis and fully automated radiosynthesis. *Appl. Radiat. Isot.* **2011**, *69*, 862−868.

(44) Mutschler, E. *Arzneimittelwirkungen*; Wissenschaftliche Verlagsgesellschaft mbH: Stuttgart, Germany, 1996; pp 20−36.

(45) Zang, W.; Oya, S.; Kung, M. P.; Hou, C.; Maier, D. L.; Kung, H. F. F-18 polyethyleneglycol stilbenes as PET imaging agents targeting Aβ aggregates in the brain. *Nucl. Med. Biol.* **2005**, *32*, 799−809.

(46) Zang, W.; Kung, M. P.; Oya, S.; Hou, C.; Kung, H. F. ^{18}F-Labeled styrylpyridines as PET agents for amoloid plaque imaging. *Nucl. Med. Biol.* **2007**, *34*, 89−97.

(47) Wu, Z.; Li, Z. B.; Chen, K.; Cai, W.; He, L.; Chin, F. T.; Li, F.; Chen, X. MicroPET of tumor integrin $\alpha_\nu\beta_3$ expression using ^{18}F-labeld PEGylated tetrameric RGD peptide (^{18}F-FPRGD4). *J. Nucl. Med.* **2007**, *48*, 1536−1544.

(48) Chen, X.; Park, R.; Hou, Y.; Khankaldyyan, V.; Gonzales-Gomez, I; Tohme, M; Bading, J. R.; Laug, W. E.; Conti, P. S. MicroPET imaging of brain tumor angiogenesis with ^{18}F-labeled PEGylated RGD peptide. *Eur. J. Nucl. Med. Mol. Imaging* **2004**, *31*, 1081−1089.

(49) Pirard, B.; Matter, H. Matrix metalloproteinase target family landscape: a chemometrical approach to ligand selectivity based on protein binding site analysis. *J. Med. Chem.* **2006**, *49*, 51−69.

(50) Lopez, M.; Salmon, A. J.; Supuran, C. T.; Poulsen, S. A. Carbonic anhydrase inhibitors developed through "click tailing". *Curr. Pharm. Des.* **2010**, *16*, 3277−3287.

(51) Glaser, M.; Årstad, E. Click labeling with 2-[18F]fluoroethylazide for positron emission tomography. *Bioconjugate Chem.* **2007**, *18*, 989−993.

(52) Maschauer, S.; Prante, O. A series of 2-O-trifluoromethylsulfonyl-D-mannopyranosides as precursors for concomitant ^{18}F-labeling and glycosylation by click chemistry. *Carbohydr. Res.* **2009**, *344*, 753−761.

(53) Dalvie, D. K.; Kalgutkar, A. S.; Khojasteh-Bakht, S. C.; Obach, R. S.; O'Donnell, J. P. Biotransformation reactions of five-membered aromatic heterocyclic rings. *Chem. Res. Toxicol.* **2002**, *15*, 269−299.

(54) Horne, W. S.; Yadav, M. K.; Stout, C. D.; Ghadiri, M. R. Heterocyclic peptide backbone modifications in an alpha-helical coiled coil. *J. Am. Chem. Soc.* **2004**, *126*, 15366−15367.

(55) Appendino, G.; Bacchiega, S.; Minassi, A.; Cascio, M. G.; De Petrocellis, L.; Di Marzo, V. The 1,2,3-triazole ring as a peptide-olefinomimetic element: discovery of click vanilloids and cannabinoids. *Angew. Chem., Int. Ed.* **2007**, *46*, 9312−9315.

(56) Vatmurge, N. S.; Hazra, B. G.; Pore, V. S.; Shirazi, F.; Deshpande, M. V.; Kadreppa, S.; Chattopadhyay, S.; Gonnade, R. G. Synthesis and biological evaluation of bile acid dimmers linked with 1,2,3-triazole and bis-beta-lactam. *Org. Biomol. Chem.* **2008**, *6*, 3823−3830.

(57) Macleod, F.; Lang, S.; Murphy, J. A. The 2-(2-azidoethyl)-cycloalkanone strategy for bridged amides and medium-sized amine derivatives in the Aubé−Schmidt reaction. *Synlett* **2010**, 529−534.

(58) Huang, W.; Meng, Q.; Suzuki, K.; Nagase, H.; Brew, K. Mutational study of the amino-terminal domain and human tissue inhibitor of metalloproteinases 1 (TIMP-1) locates an inhibitory region for matrix metallo proteinases. *J. Biol. Chem.* **1997**, *272*, 22086−22091.

(59) Prante, O.; Hocke, C.; Löber, S.; Hübner, H.; Gmeiner, P.; Kuwert, T. Tissue distribution of radioiodinated FAUC113: assess-

ment of a pyrazolo[1,5-*a*]pyridine-based dopamine D4 receptor radioligand candidate. *Nuklearmedizin* **2006**, *45*, 41−48.

(60) Schäfers, K. P.; Reader, A. J.; Kriens, M.; Knoess, C.; Schober, O.; Schäfers, M. Performance evaluation of the 32-module quadHIDAC small animal PET scanner. *J. Nucl. Med.* **2005**, *46*, 996−1004.